Acta Cryst B
STRUCTURAL SCIENCE
CRYSTAL ENGINEERING
MATERIALS
ISSN 2052-5206

Compression of glycolide-h_4 to 6 GPa

Ian B. Hutchison,[a] Craig L. Bull,[b]* William G. Marshall,[b]‡ Simon Parsons,[c] Andrew J. Urquhart[d] and Iain D. H. Oswald[a]*

[a]Strathclyde Institute of Pharmacy and Biomedical Sciences, University of Strathclyde, 161 Cathedral Street, Glasgow, G40RE, UK, [b]ISIS Neutron and Muon Source, Science and Technology Facilities Council, Rutherford Appleton Laboratory, Harwell, Didcot OX11 0QX, UK, [c]School of Chemistry and Centre for Science at Extreme Conditions, The University of Edinburgh, Kings Buildings West Mains Road, Edinburgh, EH9 3FJ, UK, and [d]Department of Micro- and Nanotechnology, Technical University of Denmark, Ørsteds Plads, Building 345Ø, Lyngby, 2800 Kgs., Denmark. *Correspondence e-mail: craig.bull@stfc.ac.uk, iain.oswald@strath.ac.uk

Received 15 August 2017
Accepted 26 October 2017

Edited by A. Katrusiak, Adam Mickiewicz University, Poland

‡ 1963–2015

Keywords: high pressure; polymorphism; phase transition; neutron diffraction; hydrogenated.

CCDC references: 1582353; 1582354; 1582355; 1582356; 1582357

Supporting information: this article has supporting information at journals.iucr.org/b

This study details the structural characterization of glycolide-h_4 as a function of pressure to 6 GPa using neutron powder diffraction on the PEARL instrument at ISIS Neutron and Muon source. Glycolide-h_4, rather than its deuterated isotopologue, was used in this study due to the difficulty of deuteration. The low background afforded by zirconia-toughened alumina anvils nevertheless enabled the collection of data suitable for structural analysis to be obtained to a pressure of 5 GPa. Glycolide-h_4 undergoes a reconstructive phase transition at 0.15 GPa to a previously identified form (II), which is stable to 6 GPa.

1. Introduction

The study of molecular materials at high pressure has been a fruitful area for structural science with many compounds showing significant structural changes at elevated pressures (Zakharov, Seryotkin *et al.*, 2016; Zakharov, Goryainov & Boldyreva, 2016; Hobday *et al.*, 2016; Fabbiani *et al.*, 2007; Zakharov & Boldyreva, 2014; Moggach *et al.*, 2008; Wood *et al.*, 2008). High-pressure crystallographic techniques have been used to identify new polymorphs and solvates which are unknown under ambient conditions (Moggach *et al.*, 2008; Olejniczak *et al.*, 2016; Oswald & Pulham, 2008; Oswald *et al.*, 2008). In particular, we have been investigating the phenomenon of solid-state pressure-induced polymerization and the role polymorphism has on the reaction product (Johnston *et al.*, 2014; Marshall *et al.*, 2015; Oswald & Urquhart, 2011). There have been a number of spectroscopic studies (Murli & Song, 2010; Bini *et al.*, 2012; Ceppatelli *et al.*, 2000; Chelazzi *et al.*, 2005; Ciabini *et al.*, 2002; Ciabini *et al.*, 2007; Santoro *et al.*, 2003; Aoki *et al.*, 1989; Kojima *et al.*, 1995; Murli *et al.*, 2012) but only a few diffraction-based studies (Jin *et al.*, 2013; Wilhelm *et al.*, 2008) that have investigated chemical reactions in a range of aromatic, olefinic materials. Recent work by Sun *et al.* (2017) has highlighted the role of neutron powder diffraction and solid-state NMR to elucidate the pathways to various products from the compression of acetylene depending on the pressure achieved. Ring systems have been investigated using spectroscopy and observed to undergo chemical reactions, *e.g.* carosine (Murli *et al.*, 2012) and L,L-lactide (Ceppatelli *et al.*, 2011). In the solid-state, L,L-lactide is stable up to 17 GPa which was the highest pressure achieved in the study but under high-pressure and high-temperature conditions begins to polymerize.

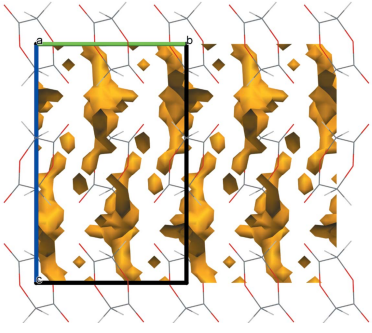

Glycolide ($C_4H_4O_4$; Scheme 1) is the pre-cursor to poly-(glycolic acid) and undergoes a ring-opening polymerization to the polymeric product under ambient pressure (Dechy-Cabaret *et al.*, 2004). We previously investigated glycolide at high pressure, revealing the formation of a new high-pressure polymorph [form (II); *Pbca*] between 0.4 and 0.58 GPa which was unusual in being recoverable at ambient pressure and accessible on a gram scale when prepared using a large volume press (Hutchison *et al.*, 2015). The transition to form (II) is reconstructive and the molecule shows a significant conformational change to become disordered about an inversion centre. In this paper, we will discuss the changes in the crystal structure of glycolide from ambient pressure to 6 GPa using high-pressure neutron powder diffraction.

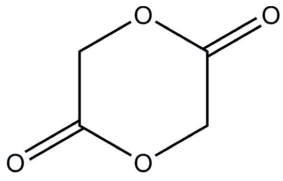

Scheme 1

2. Experimental

2.1. High-pressure neutron powder diffraction

High-pressure neutron powder diffraction data were collected using the PEARL diffractometer at the UK spallation neutron source, ISIS, located at the STFC Rutherford Appleton Laboratory (Bull *et al.*, 2016). Glycolide-h_4 was purchased from Sigma–Aldrich and recrystallized from a saturated acetone solution before being ground at ambient temperature. An encapsulated null-scattering titanium–zirconium gasket (Marshall & Francis, 2002) and one of the zirconia-toughened alumina (ZTA) anvils were cooled to 263 K under a nitrogen purge before loading the gasket with glycolide, lead (for use as a pressure marker) (Schulte & Holzapfel, 1995; Vohra & Ruoff, 1990; Mao *et al.*, 1990) and a 1:1 mixture of pentane-d_{12} and isopentane-d_{12} as a pressure-transmitting medium (PTM) (Klotz *et al.*, 2009). Cooling the gasket and anvil was necessary because both components of the PTM are highly volatile; the nitrogen purge minimized condensation of atmospheric moisture onto the gasket/anvil assembly. The gasket/anvil assembly was quickly inserted into a Paris–Edinburgh V3 press before applying 6 tonnes of load to ensure the gasket was sealed but not applying significant pressure to the sample. The time-of-flight (TOF) neutron powder diffraction data were collected and reduced using procedures outlined in our previous work (Johnston *et al.*, 2014). Data suitable for structure refinement were collected over a period of 8 h in increments of ~1 GPa interspersed with shorter runs of 2–4 h to allow monitoring of the of the unit-cell parameters.

The data were analysed with *TOPAS-Academic* software (Coelho, 2012). The initial pattern, at approximately ambient pressure, was consistent with glycolide form (I) (Fig. 1). Patterns collected above 0.15 GPa indicated that the sample had transformed to form (II). Only the data for form (II) was suitable for Rietveld refinement. For these refinements a model defined using a Z-matrix with all atoms set to 0.5 occupancy was used to account for atoms generated by the inversion symmetry. The use of the Z-matrix was a convenient way of describing the molecular geometry especially in the disordered form (II). The starting model for the high pressure structure refinements was taken from our previously reported X-ray study (Hutchison *et al.*, 2015). Torsional angles were allowed to refine and showed the puckered nature of the rings under pressure. The final refined unit-cell parameters are listed in Table S1.

Fig. 1 shows indicative patterns below and above the phase transition which shows a change in diffraction intensity between the two patterns. The intensity of the glycolide signal increased by ~25% over the course of the form (I)-to-(II) transition, which suggests that the initial sample contained an amorphous component, which recrystallized into form (II) on increasing the pressure.

2.2. PIXEL calculations

Form (II) of glycolide is an orthorhombic structure with the molecule disordered over an inversion centre. PIXEL calculations were carried out on an ordered model in $P2_12_12_1$. Electron densities were calculated using *Gaussian*09 (Frisch *et al.*, 2009) with the MP2/6-31G** basis set. The PIXEL results were analysed using *processPIXEL* (Bond, 2014).

2.3. Other programs

Pucker (Gould *et al.*, 1995) was used to analyse the conformational changes in the molecule as a function of pressure. *EosFit7.0Gui* (Angel *et al.*, 2014) was used to determine the equation of state of form (II) of glycolide.

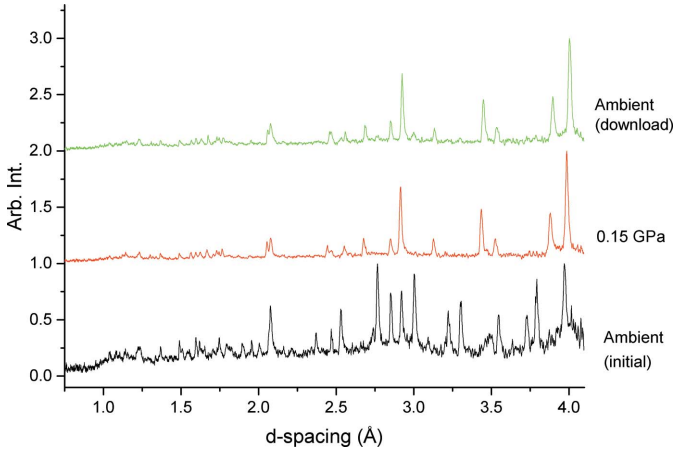

Figure 1
Normalized data for the compression of glycolide-h_4 at selected pressures: ambient pressure [form (I); $P2_1/n$]; 0.15 GPa [form (II); *Pbca*]; and decompression to ambient pressure showing retention of form (II) to ambient pressure which is in-line with our previous seeding experiment (Hutchison *et al.*, 2015). The drop-off in intensity due to the incoherent scattering of the hydrogen atoms can clearly be observed at ~1.0 Å. Rietveld fits of the data can be found in Fig. S1.

Mercury CSD 2.0 (Macrae *et al.*, 2008) was used to visualize the structures and in the production of the figures.

3. Results and discussion

3.1. Effect of pressure on glycolide-h_4

Form (I) of glycolide crystallizes in space group $P2_1/n$ with $Z' = 2$. The molecules show conformations that are mixture of twist–boat and boat conformation (Table 1). PIXEL calculations indicate that the most important intermolecular interaction is between the carbonyl groups (−34.9 kJ mol^{-1}) (Hutchison *et al.*, 2015). These types of interaction have been extensively studied by Allen *et al.* (1998) and shown to be as competitive as hydrogen bonds. The structure possesses anti-parallel carbonyl interactions between the independent molecules [3.1111 (16) Å, −34.9 kJ mol^{-1}, Fig. 2]. The dimers of molecules then interact through a sheared parallel interaction [3.2141 (16) Å, −14.7 kJ mol^{-1}, Fig. 2]. Both of these interactions are somewhat shorter than the average values for these interactions from the database at the time of the Allen study (3.33 and 3.45 Å for the anti-parallel and shear-parallel respectively). The C═O···C angles (107.50° and 61.28°) are at the high end of the distributions observed by Allen *et al.* (1998); however, their study showed that the shear motif tends to occur between molecules exhibiting π-stacking. The lack of π stacking in the present structures perhaps explains the deviation of the geometric parameters away from typical values. Allen *et al.* also computed the ideal interaction values for anti-parallel interactions using in propanone as a model compound. They used intermolecular perturbation theory with varying intermolecular distance and demonstrated that an ideal separation is 3.02 Å and angle of 90–91° (−22 kJ mol^{-1}).

Our previous work in a diamond anvil cell demonstrated that on compression of form (I), a reconstructive phase transition occurs at 0.41 GPa to form (II) (*Pbca*). We noted at the time that particle size is an important factor in the speed of transition *i.e.* a powdered sample underwent a polymorphic transition more rapidly than larger crystallites. From our neutron diffraction experiments, in this study, the phase transition to form (II) was observed to occur by 0.15 GPa which is lower than previously identified. The use of the powder in this experiment will have contributed to the lower transition pressure by reducing the kinetic barrier that the single-crystal imposes allowing for a more accurate determination of the phase transformation pressure.

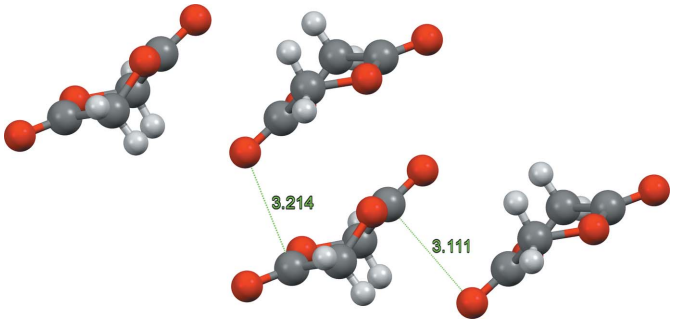

Figure 2
Monoclinic crystal structure of form (I) of glycolide showing the carbonyl anti-parallel interaction [3.1111 (16) Å] and interaction between the dimers [3.2141 (16) Å].

Table 1
Ring puckering analysis for glycolide under variable pressure†.

	Percentage component			
	Chair	Twist–boat	Boat	Relative conformational energy (kJ mol^{-1})
Form (I) Mol. 1; 0 GPa	1	38	61	0
Form (I) Mol. 2; 0 GPa	0	42	58	0.48651
Form (II); 0 GPa	16	51	33	36.10719
0.4 GPa	6	65	29	42.66359
1.8 GPa	12	71	17	16.98935
2.6 GPa	7	74	19	35.63827
4.0 GPa	8	49	43	20.43952
5.0 GPa	16	41	43	24.38591

† The analysis was performed using *Pucker* (Gould *et al.*, 1995) with the $P2_12_12_1$ description of the structure to allow for the input of one molecule with refined atomic positions. Single-point energy calculations were performed in *Gaussian*09 (Frisch *et al.*, 2009) with the MP2/6-31G** basis set.

Form (II) compresses monotonically up to a pressure of 5.89 GPa (Fig. 3). Refinement of the unit-cell parameters shows a decrease in the unit-cell volume of 20% between 0.4 and 5.9 GPa. The bulk modulus determined for form (II) of

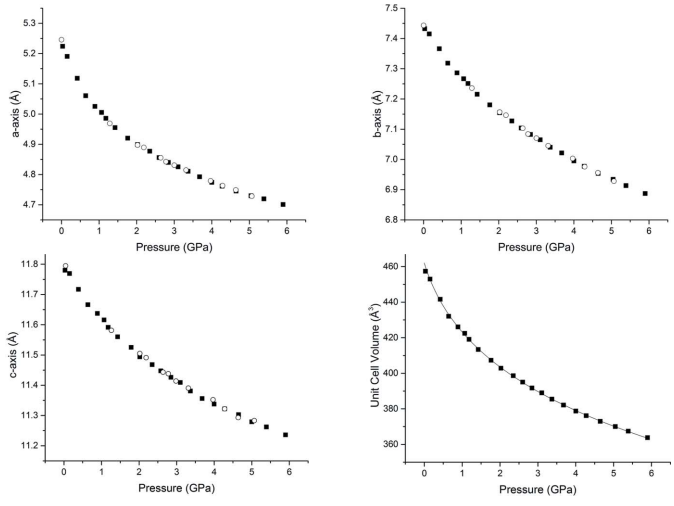

Figure 3
The compression of the unit-cell parameters of form (II) of glycolide. The black squares representing the compression and the hollow circles represent the parameters on decompression. No hysteresis is observed. The standard deviations for the parameters are smaller than the symbols. Equation of state for form (II) glycolide-h_4 (bottom right). The line represents the fit to the data using a third-order Birch–Murnaghan equation of state [V_0 of 461.9 (8) Å^3, K = 6.6 (4) GPa, K' = 14.0 (7)]. The pressure variation of the individual unit-cell parameters have been fitted. For the axial cell parameters, this analysis modelled the pressure variation of $\ln a$, $\ln b$ and $\ln c$ by means of a low-order (typically quadratic) polynomials. Using this simple model, least-squares fits of the form (II) unit-cell parameters yielded the following values for the initial compressibilities β_a = 0.0468 (20) GPa^{-1}, β_b = 0.0247 (7) GPa^{-1} and β_c = 0.0162 (5) GPa^{-1}, where $\beta_a = -(1/a)(\partial a/\partial p)$.

glycolide is 6.6 (4) GPa with a V_0 of 461.9 (8) Å^3, K' = 14.0 (7) using a third-order Birch–Murnaghan equation of state (Fig. 3) which is in line with other organic materials lacking hydrogen bonding, *e.g.* rubrene K = 8.2 (8) GPa and K' = 9.4 (9) (Bergantin *et al.*, 2014), anthracene K = 8.4 (6) GPa and K' = 6.3 (4) (Oehzelt *et al.*, 2006), and a little softer than extensively hydrogen-bonded organic solids, *e.g.* L-alanine is K = 13.4 (7) GPa and K' = 7.0 (3) (Funnell *et al.*, 2011). The compression of the unit cell is anisotropic with the *a* axis showing greatest compression (10%) followed by the *b* axis (7.3%) and the *c* axis (4.6%). As the structure is orthorhombic, the principal axes of the strain tensor are aligned with the unit cell axes.

As in form (I), the molecules in form (II) adopt a mixture of a twist–boat and boat conformation, but with a greater proportion of the latter (Table 1). As the pressure applied reaches 4 and 5 GPa the conformation tends towards the boat conformation which is energetically closer to the form (I) conformations.

Form (II) is a layered structure with the layers extending over the *ab* plane (Fig. 4). Glycolide does not possess any hydrogen-bond donating groups and hence relies on CH···O, carbonyl and van der Waals interactions for stabilization. Form (II) does not possess the carbonyl interactions of form (I) instead opting for a configuration whereby the molecules interact *via* a herringbone motif where the ether group is orientated towards the face of the neighbouring molecule (−23.4 kJ mol^{-1}, current work). From the packing arrangement in Fig. 4, the central molecule interacts with its four nearest neighbours within the *ab* layer [Fig. 4(*a*); red and black dotted lines] through interactions that are largely Coulombic (−21.5 and −19.5 kJ mol^{-1}) and dispersive (−21.4 and −16.7 kJ mol^{-1}; interactions 1 and 2; Table S3). The use of PIXEL calculations allow us to map out the intermolecular potentials for all the close interactions in the crystal structure as distances are compressed. From these observations it can be noted that interactions 1 and 2 lie at the bottom of this potential at an ideal distance at the lowest pressure of 0.4 GPa.

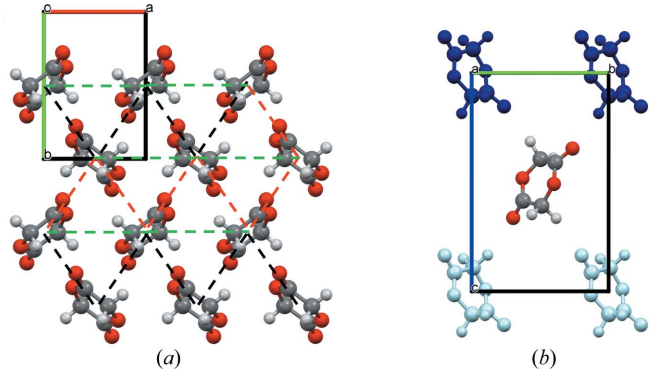

Figure 4
Form (II) of glycolide viewed down (*a*) the *c* axis showing how the *ab* layers are arranged with the two strongest interactions indicated by red (interaction 1) and black (interaction 2) dotted lines and the third strongest by the green (interaction 3) dotted lines; (*b*) the fourth (interaction 4; dark blue) and fifth (interaction 5; light blue) strongest interactions in form (II).

These interactions becoming immediately less stabilizing as they are compressed (Figs. 5 and 6).

As noted from the compression of the cell parameters the *a* axis is the most compressible direction which is parallel to interaction 3 (green dotted line). The PIXEL calculations show that of the three most energetic interactions, this contact has the shallowest potential, and it is only above 2.5 GPa that the magnitude of the interaction energy begins to decrease. This suggests that by analysing the intermolecular potentials in this way, we may be able to understand which directions in the crystal structure are the most compressible. This would be particularly useful in lower symmetry crystals where the principal axes of strain tensor do not correspond to the cell directions.

Interactions 4 and 5 are formed between molecules in different layers and they interact in a slightly different way. (Fig. 4a) The molecules involved in these interactions are aligned such that there is an almost linear interaction between C—H···OC (170°), compared with interactions 1 and 2 where the molecules interact side-on. We believe that this has an impact on the compression of the cell and the energies of the interactions. The *c* axis is the least compressible despite the voids being concentrated between the *ab* layers. As the nearest point of contact the linear nature of the C—H···OC interaction is likely to be providing resistance to the compression and will be the major contributor to the repulsion term (Fig. 6). At the same time there is an equal stabilization effect as the molecules come closer together through more negative Coulombic, polarization and dispersive energy contributions to the total energy of the interaction hence the energies of the interactions remain relatively constant over the compression.

Due to the limitations of the pressure capabilities of the pressure-transmitting media it was not possible to compress further; however, Raman data collected on a sample to 8.03 GPa show little change apart from a pressure shift

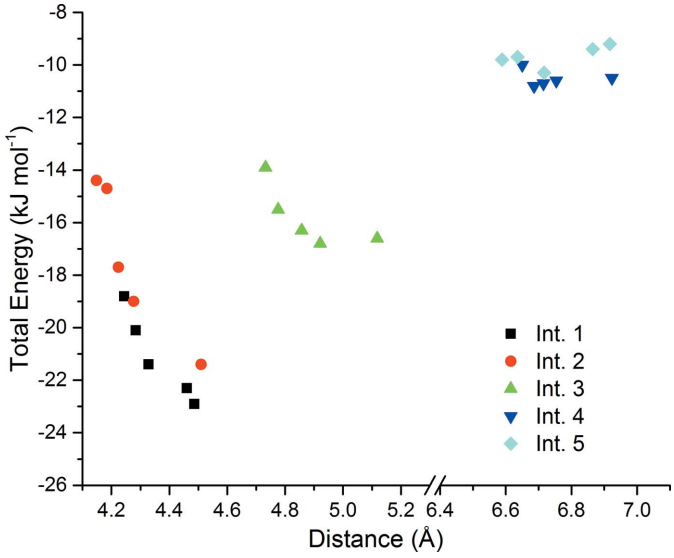

Figure 5
Interaction energies for the top five interactions in glycolide-h$_4$ form (II). Interactions 1–3 are observed between molecules in the *ab* layers.

(Fig. S2). We monitored the sample at this pressure for eight days but the spectra are not substantially different. The sample was compressed further to 10.4 GPa and it showed chemical stability of glycolide to this pressure. As a reference, L,L-lactide is stable to 17.3 GPa with no signs of polymerizing.

3.2. Decompression behaviour

Overall, from our diffraction experiment glycolide remains molecular in nature up to 6 GPa with evidence of stability to 10 GPa from Raman data (Fig. S2). There is no evidence of any polymerization occurring which was part of our hypothesis for looking at monomeric compounds under pressure. Our previous work on acrylic and methacrylic acid (Johnston *et al.*, 2014; Marshall *et al.*, 2015) demonstrated that polymerization could occur on decompression but on release of pressure form (II) persists to ambient pressure, although due to the constraints of allocated beamtime the longevity of this form is unknown (Figs. 1 and 7). From our previous work we observed that the crystals from a seeded solution of the high-pressure form lasted 12 days (Hutchison *et al.*, 2015).

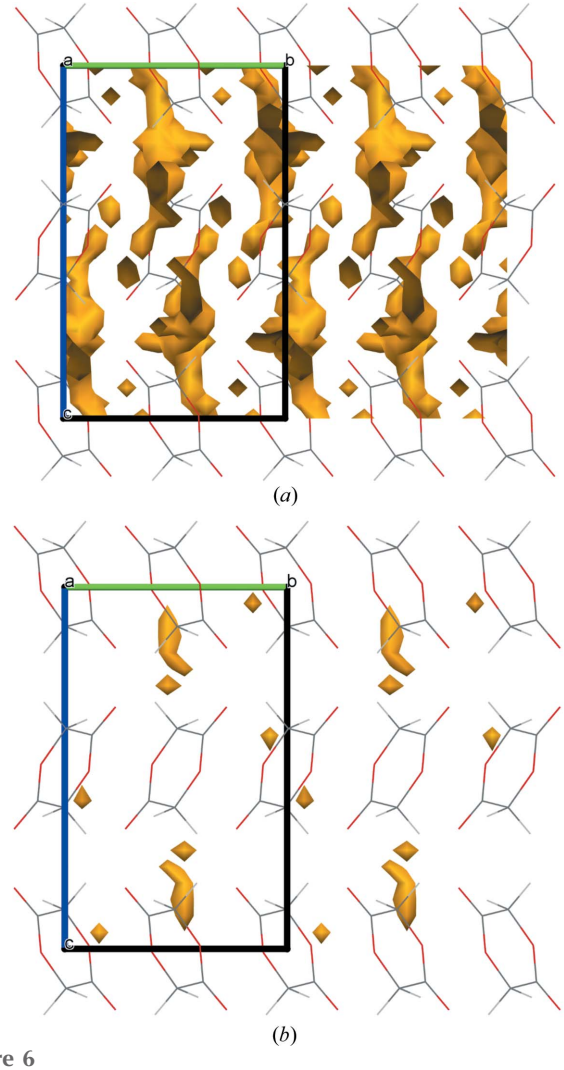

Figure 6
The void space in the crystal structures at (*a*) 0.4 GPa and (*b*) 5.0 GPa calculated from geometry optimized structure due to the disorder in the model. The probe radius was set to 0.2 Å and the grid spacing set to 0.5 Å giving a void volume of 5.3% of unit cell volume at 0.4 GPa and 0.4% at 5.0 GPa. Notably, the last void space remaining is that observed between the layers along the *c* axis.

3.3. Effect of hydrogenation on diffraction pattern

The disadvantage of investigating hydrogenous samples using neutron powder diffraction comes from the incoherent scattering of hydrogen which causes the powder diffraction pattern to have a higher and noisier background (Wilson *et al.*, 2014). In general, to overcome this, deuteration or single-crystal studies are performed; however, in this study neither of these options was available to us. Hydrogen-containing samples have been investigated using neutron powder diffraction in a wide range of areas from materials science to chemical reactivity and have been the subject of a number of reviews (Weller *et al.*, 2009; Wilson *et al.*, 2014; Hansen & Kohlmann, 2014). One of the over-riding requirements is that high-flux instruments were required for the data collections (Murshed & Kuhs, 2009; Murshed *et al.*, 2010). High-pressure neutron diffraction on hydrogenated materials has been conducted before on methane/CO_2 gas hydrates (Staykova *et al.*, 2003) and brucite (Horita *et al.*, 2010) but the added sample environment can add further complications, *e.g.* even higher backgrounds. One of the major developments at PEARL in recent years is the use of a neutron transparent ceramic (a ZTA anvil), an alternative anvil material to the previously used tungsten carbide (WC) (Bull *et al.*, 2016). At higher TOF (and longer *d*-spacing), the neutron transparency of the anvils allows a doubling of the signal compared with WC anvils with significantly reduced contamination in the diffraction pattern from the anvil material itself (Bull *et al.*, 2016). By using these anvils, we have been able to collect data of sufficient quality on this weakly scattering solid for Rietveld refinement of the structure (Fig. S1); the patterns shown in Fig. 1 were collected for 4 h. The data collection time of 8 h to obtain a pattern for Rietveld refinement typically compares with 4 h for a fully deuterated molecular organic solid. This is

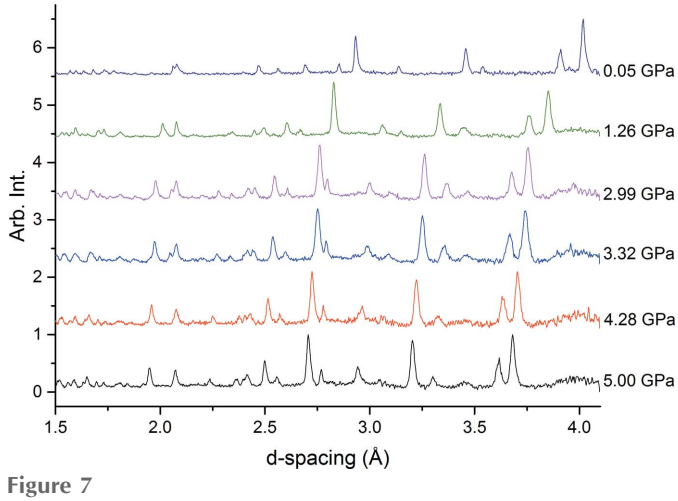

Figure 7
The decompression of glycolide from 5 GPa to ambient pressure showing the recovery of orthorhombic form (II).

not ideal with limited allocations of beamtime; however, the advantages of being able to use a hydrogenated material without having to deuterate are significant. In particular, in cases where materials have altered properties in either their hydrogenated or deuterated form (highlighted below) or when the synthesis of deuterated materials is problematic such as is the case for glycolide.

The role of deuterium substitution may not have been systematically investigated but there are a number of studies that have identified changes in the phase behaviour of solids when this has occurred. This is a particularly important question if both neutron and X-ray techniques are being used to investigate the solid-state behaviour of materials. Two examples of the effects of deuteration on small molecules are observed with pyridine (Crawford *et al.*, 2009) and in acridine (Kupka *et al.*, 2012). The deuteration effect in pyridine was observed during a screen for new polymorphs which had been instigated by crystal structure predictions that showed a number of potential polymorphs equal in energy to the known $Z' = 4$ structure but with $Z' = 1$. All outcomes from the use of pyridine-h_5 in the crystallizations were the known form. Only when pyridine-d_5 was used did the authors isolate a new polymorph either from the pure compound or from a solution of pyridine-d_5 in pentane. The authors rationalized that the saturation solubility of pyridine-d_5 in pentane permitted the crystallization below the phase transition and hence the identification of the thermodynamically stable form at low temperature. At the same time, the high-resolution low-temperature neutron diffraction as well as high-pressure neutron diffraction measurements were being conducted, the latter being the only method by which both the d_5 and h_5 forms could crystallize in the $Z' = 1$ structure.

The effect of deuteration on acridine was observed on crystallization from acetone. Kupka *et al.* (2012) observed that either form (II) (acridine-h_9) or form (III) (acridine-d_9) could be crystallized from acetone as the pure polymorphs. In form (II) all the molecules are associated *via* a dimer with CH$\cdots$N interactions whilst form (III) is a $Z' = 2$ structure, where molecules are linked through dimer interactions as well as a single C—D$\cdots$N interaction. The authors investigated the intermolecular potentials for C—D$\cdots$N and suggested that the substitution favoured the formation of additional C—D$\cdots$N interactions. For a recent review of the effects of deuteration on organic systems as well as the effects of deuterated solvents on crystallization, readers are directed to a review by Merz & Kupka (2015).

4. Concluding remarks

We have shown in this paper that we have been able to investigate the changes that occur in glycolide-h_4 to 6 GPa in the Paris–Edinburgh press. The reconstructive nature of the phase transition at 0.15 GPa necessitated the use of powder diffraction for sample analysis. The advantage of larger sample size afforded by the Paris–Edinburgh press and non-invasive nature of neutron radiation (over synchrotron source) made neutron powder diffraction the method of choice for our analysis. The use of hydrogenated material is a problem; however, the experiment has been enabled by the use of zirconia-toughened alumina anvils that possess a significantly better neutron transparency compared with traditional tungsten carbide anvils. In this study we have observed that the phase transition to a previously identified high-pressure form [form (II)] but at lower pressures than observed previously. This has been attributed to the use of the powdered form of glycolide in this experiment compared with previous work allowing for a rapid transition between the two phases. We have verified the existence and recovery of form (II) under ambient conditions but due to time constraints were unable to assess its longevity at ambient pressure.

Acknowledgements

The authors would like to thank Paul Henry and Alastair Florence for useful discussions.

Funding information

The authors would like to thank the Science and Technologies Facilities Council for the provision of beamtime (RB1510085) and the EPSRC for the provision of the PhD (IBH) and fellowship for IDHO (EP/N015401/1). The authors would also like to thank the Leverhulme Trust for the grant RPG2012-598.

References

Allen, F. H., Baalham, C. A., Lommerse, J. P. M. & Raithby, P. R. (1998). *Acta Cryst.* B**54**, 320–329.
Angel, R. J., Alvaro, M. & Gonzalez-Platas, J. (2014). *Z. Kristallogr.* **229**, 405–419.
Aoki, K., Kakudate, Y., Yoshida, M., Usuba, S. & Fujiwara, S. (1989). *J. Chem. Phys.* **91**, 778–782.
Bergantin, S., Moret, M., Buth, G. & Fabbiani, F. P. A. (2014). *J. Phys. Chem. C*, **118**, 13476–13483.
Bini, R., Ceppatelli, M., Citroni, M. & Schettino, V. (2012). *Chem. Phys.* **398**, 262–268.
Bond, A. D. (2014). *J. Appl. Cryst.* **47**, 1777–1780.
Bull, C. L., Funnell, N. P., Tucker, M. G., Hull, S., Francis, D. J. & Marshall, W. G. (2016). *High Pressure Res.* **36**, 493–511.
Ceppatelli, M., Frediani, M. & Bini, R. (2011). *J. Phys. Chem. B*, **115**, 2173–2184.
Ceppatelli, M., Santoro, M., Bini, R. & Schettino, V. (2000). *J. Chem. Phys.* **113**, 5991–6000.
Chelazzi, D., Ceppatelli, M., Santoro, M., Bini, R. & Schettino, V. (2005). *J. Phys. Chem. B*, **109**, 21658–21663.
Ciabini, L., Santoro, M., Bini, R. & Schettino, V. (2002). *J. Chem. Phys.* **116**, 2928–2935.
Ciabini, L., Santoro, M., Gorelli, F. A., Bini, R., Schettino, V. & Raugei, S. (2007). *Nat. Mater.* **6**, 39–43.
Coelho, A. (2012). *TOPAS-Academic.* Version 5. Coelho Software, Brisbane, Australia.
Crawford, S., Kirchner, M. T., Blaser, D., Boese, R., David, W. I. F., Dawson, A., Gehrke, A., Ibberson, R. M., Marshall, W. G., Parsons, S. & Yamamuro, O. (2009). *Angew. Chem. Int. Ed.* **48**, 755–757.
Dechy-Cabaret, O., Martin-Vaca, B. & Bourissou, D. (2004). *Chem. Rev.* **104**, 6147–6176.
Fabbiani, F. P. A., Allan, D. R., David, W. I. F., Davidson, A. J., Lennie, A. R., Parsons, S., Pulham, C. R. & Warren, J. E. (2007). *Cryst. Growth Des.* **7**, 1115–1124.

Frisch, M. J. *et al.* (2009). *Gaussian* 09, Revision B.01. Gaussian Inc., Wallingford, CT, USA.
Funnell, N. P., Marshall, W. G. & Parsons, S. (2011). *CrystEngComm*, **13**, 5841–5848.
Gould, R. O., Taylor, P. & Thorpe, M. (1995). *Pucker.* Version 7.7.95. University of Edinburgh, Scotland.
Hansen, T. C. & Kohlmann, H. (2014). *Z. Anorg. Allg. Chem.* **640**, 3044–3063.
Hobday, C. L., Marshall, R. J., Murphie, C. F., Sotelo, J., Richards, T., Allan, D. R., Duren, T., Coudert, F. X., Forgan, R. S., Morrison, C. A., Moggach, S. A. & Bennett, T. D. (2016). *Angew. Chem. Int. Ed.* **55**, 2401–2405.
Horita, J., dos Santos, A. M., Tulk, C. A., Chakoumakos, B. C. & Polyakov, V. B. (2010). *Phys. Chem. Miner.* **37**, 741–749.
Hutchison, I. B., Delori, A., Wang, X., Kamenev, K. V., Urquhart, A. J. & Oswald, I. D. H. (2015). *CrystEngComm*, **17**, 1778–1782.
Jin, H. J., Plonka, A. M., Parise, J. B. & Goroff, N. S. (2013). *CrystEngComm*, **15**, 3106–3110.
Johnston, B. F., Marshall, W. G., Parsons, S., Urquhart, A. J. & Oswald, I. D. H. (2014). *J. Phys. Chem. B*, **118**, 4044–4051.
Klotz, S., Chervin, J. C., Munsch, P. & Le Marchand, G. (2009). *J. Phys. D*, **42**, 7.
Kojima, Y., Matsuoka, T., Sato, N. & Takahashi, H. (1995). *J. Polym. Sci. Polym. Chem.* **33**, 2935–2940.
Kupka, A., Vasylyeva, V., Hofmann, D. W. M., Yusenko, K. V. & Merz, K. (2012). *Cryst. Growth Des.* **12**, 5966–5971.
Macrae, C. F., Bruno, I. J., Chisholm, J. A., Edgington, P. R., McCabe, P., Pidcock, E., Rodriguez-Monge, L., Taylor, R., van de Streek, J. & Wood, P. A. (2008). *J. Appl. Cryst.* **41**, 466–470.
Mao, H. K., Wu, Y., Shu, J. F., Hu, J. Z., Hemley, R. J. & Cox, D. E. (1990). *Solid State Commun.* **74**, 1027–1029.
Marshall, W. G. & Francis, D. J. (2002). *J. Appl. Cryst.* **35**, 122–125.
Marshall, W. G., Urquhart, A. J. & Oswald, I. D. H. (2015). *J. Phys. Chem. B*, **119**, 12147–12154.
Merz, K. & Kupka, A. (2015). *Cryst. Growth Des.* **15**, 1553–1558.
Moggach, S. A., Parsons, S. & Wood, P. A. (2008). *Crystallogr. Rev.* **14**, 143–183.
Murli, C., Mishra, A. K., Thomas, S. & Sharma, S. M. (2012). *J. Phys. Chem. B*, **116**, 4671–4676.
Murli, C. & Song, Y. (2010). *J. Phys. Chem. B*, **114**, 9744–9750.
Murshed, M. M. & Kuhs, W. F. (2009). *J. Phys. Chem. B*, **113**, 5172–5180.
Murshed, M. M., Schmidt, B. C. & Kuhs, W. F. (2010). *J. Phys. Chem. A*, **114**, 247–255.
Oehzelt, M., Aichholzer, A., Resel, R., Heimel, G., Venuti, E. & Della Valle, R. G. (2006). *Phys. Rev. B*, **74**, 104103.
Olejniczak, A., Krukle-Berzina, K. & Katrusiak, A. (2016). *Cryst. Growth Des.* **16**, 3756–3762.
Oswald, I. D. H., Hamilton, A., Hall, C., Marshall, W. G., Prior, T. J. & Pulham, C. R. (2008). *J. Am. Chem. Soc.* **130**, 17795–17800.
Oswald, I. D. H. & Pulham, C. R. (2008). *CrystEngComm*, **10**, 1114–1116.
Oswald, I. D. H. & Urquhart, A. J. (2011). *CrystEngComm*, **13**, 4503–4507.
Santoro, M., Ciabini, L., Bini, R. & Schettino, V. (2003). *J. Raman Spectrosc.* **34**, 557–566.
Schulte, O. & Holzapfel, W. B. (1995). *Phys. Rev. B*, **52**, 12636–12639.
Staykova, D. K., Kuh, W. F., Salamatin, A. N. & Hansen, T. (2003). *J. Phys. Chem. B*, **107**, 10299–10311.
Sun, J. M., Dong, X., Wang, Y. J., Li, K., Zheng, H. Y., Wang, L. J., Cody, G. D., Tulk, C. A., Molaison, J. J., Lin, X. H., Meng, Y. F., Jin, C. Q. & Mao, H. K. (2017). *Angew. Chem. Int. Ed.* **56**, 6553–6557.
Vohra, Y. K. & Ruoff, A. L. (1990). *Phys. Rev. B*, **42**, 8651–8654.
Weller, M. T., Henry, P. F., Ting, V. P. & Wilson, C. C. (2009). *Chem. Commun.* pp. 2973–2989.
Wilhelm, C., Boyd, S. A., Chawda, S., Fowler, F. W., Goroff, N. S., Halada, G. P., Grey, C. P., Lauher, J. W., Luo, L., Martin, C. D., Parise, J. B., Tarabrella, C. & Webb, J. A. (2008). *J. Am. Chem. Soc.* **130**, 4415–4420.
Wilson, C. C., Henry, P. F., Schmidtmann, M., Ting, V. P., Williams, E. & Weller, M. T. (2014). *Crystallogr. Rev.* **20**, 162–206.
Wood, P. A., Francis, D., Marshall, W. G., Moggach, S. A., Parsons, S., Pidcock, E. & Rohl, A. L. (2008). *CrystEngComm*, **10**, 1154–1166.
Zakharov, B. A. & Boldyreva, E. V. (2014). *J. Mol. Struct.* **1078**, 151–157.
Zakharov, B. A., Goryainov, S. V. & Boldyreva, E. V. (2016). *CrystEngComm*, **18**, 5423–5428.
Zakharov, B. A., Seryotkin, Y. V., Tumanov, N. A., Paliwoda, D., Hanfland, M., Kurnosov, A. V. & Boldyreva, E. V. (2016). *RSC Adv.* **6**, 92629–92637.